OFDM Receiver for Fixed Satellite Channel

Nathalie Thomas, Marie-Laure Boucheret, Anh Tai Ho, Mathieu Dervin, and Xavier Deplancq

Abstract: **This paper proposes an orthogonal frequency division multiplexing (OFDM) waveform for the forward link of a fixed broadband satellite system. We focus on the synchronization tasks in the receiver. Our objective is to minimize the required overhead, in order to improve the spectral efficiency with regard to a single carrier waveform system. A non pilot aided algorithm is used for fine synchronization. It is preceded by a coarse synchronization stage, which relies on a limited overhead (short cyclic prefix associated to some pilots). The performance of the proposed receiver is assessed through simulation results.**

Index Terms: **Gaussian channel, orthogonal frequency division multiplexing (OFDM) receiver, synchronization.**

I. INTRODUCTION

The maximization of the spectral efficiency—and therefore the transmission capacity—is a key objective for satellite broadcasting system design. In this context characterized by very high data rates, the transition from analogical to digital systems with digital video broadcasting-satellite (DVB-S) [1] standard definition, and more recently the waveform evolution towards DVB-S2 [2] have successively allowed to bring broadcasting system capacity closer to the theoretical bounds. However, there is still room for further improvement, notably considering that the current solutions for broadcasting rely on single carrier waveforms with Nyquist shaping (e.g., through raised cosine filtering), requiring a minimum bandwidth for the receiver to perform properly with acceptable complexity. For example, DVB-S2 waveform specifies a minimum roll-off factor of 0.2 for the waveform shaping, which means that the system capacity is reduced by 20% in comparison with a theoretical solution where the occupied bandwidth would equal the symbol rate.

We propose in this paper to investigate orthogonal frequency division multiplexing (OFDM) as a mean to improve the spectral efficiency of satellite broadcasting systems. The underlying idea is that the waveform shaping is not as bandwidth consuming in an OFDM multiplex involving narrow orthogonal carriers, as it is in a single carrier system for an equivalent symbol rate. Though, OFDM system spectral efficiency is affected by the regular introduction of guard intervals. These guard intervals (most often introduced under the form of cyclic prefixes) are used at first to prevent inter-symbol interferences in systems involving frequency selective channels. They are usually also used to aid the synchronization tasks in the receiver. Considering that in satellite broadcasting systems, line-of-sight mutual visibility is generally guaranteed between the satellite and the user equipment, and assuming typical terminal antenna directivity, the channel can be considered as multi-path-free. Consequently, the introduction of guard intervals between consecutive OFDM symbols is only useful for the receiver synchronization. Based on this observation, we propose to optimize the OFDM receiver architecture for this particular context characterized by a Gaussian channel, so as to minimize as much as possible the overhead due to the guard intervals, and possibly improve the system spectral efficiency in comparison with a single carrier solution.

In the literature, some complete OFDM receiver structures are proposed for fixed and mobile terrestrial channels [3], [4]. Many algorithms for timing and frequency recovery are investigated [5]–[7]. Beside, an OFDM waveform has been defined for mobile satellite applications in the recent DVB-satellite services to handhelds (SH) standard [8]. In this context, a large research effort has been made to mitigate the effect of the non linear satellite response on the OFDM signal characterized by a large power dynamic range. But, to the best of our knowledge, no OFDM waveform has been proposed for fixed satellite transmissions. We thus propose an OFDM receiver suited to the additive white Gaussian noise (AWGN) channel for the forward link of a fixed broadband satellite system. The lightest possible overhead is introduced in order to obtain a gain in spectral efficiency compared to existing single carrier fixed broadband satellite systems; DVB-S2 [2] waveform is taken as a reference for single carrier systems. The proposed receiver maintains a limited pilot overhead and short cyclic prefix in order to allow a first coarse synchronization process. Relying on this coarse synchronization, a fine synchronization process is defined, relying on non pilot aided loop structures. Both processes are optimized to use the lightest possible overhead. The performance of the proposed structure is assessed through several simulation results. This paper is organized as follows: Section II presents the problem formulation and gives some useful information regarding the synchronization impairments appearing in the considered fixed satellite transmission (impact on the received signal). Section III details the proposed receiver structure, while Section IV presents its performance. Conclusions are reported in Section V.

Manuscript received April 15, 2010.

This work was supported by Thales Alenia Space, Toulouse, France, and by the French Space Agency (CNES, Toulouse, France).

Parts of this work are presented in the 9th IEEE worshop on Signal Processing Advances for Wireless Communications (SPAWC), Recife, Brazil, July 06-09, 2008, and 16th European Signal Processing Conference (EUSIPCO), Lausanne, Switzerland, August 25-29, 2008.

N. Thomas and Marie-Laure Boucheret are with the University of Toulouse, IRIT/ENSEEIHT/TéSA, 2 rue Camichel, 31071 Toulouse, France, email: {Nathalie.Thomas, Marie-Laure.Boucheret}@n7.fr.

A. T. Ho is with INSA, 20, avenue des Buttes de Coësmes, 35043 Rennes Cedex, France, email: anh-tai.ho@insa-rennes.fr.

M. Dervin is with Thales Alenia Space, 26 av Jean François Champollion, BP 33787, 31037 Toulouse Cedex 1, France, email: mathieu.dervin@thalesalenia space.com.

X. Deplancq is with CNES, 18 av. Edouard Belin, 31401 Toulouse Cedex 4, France, email: xavier.deplancq@cnes.fr.

1229-2370/10/$10.00 © 2010 KICS

II. MODEL OF THE RECEIVED SIGNAL

A. Ideal Channel

OFDM is particularly well suited to frequency selective channels, as it relies on narrow subcarrier decomposition. Denoting N the number of sub-carriers, the ith transmitted OFDM symbol is composed of N samples that can be written:

$$Y_i(m) = \sum_{n=-\frac{N}{2}}^{\frac{N}{2}-1} X_i(n) e^{j2\pi \frac{nm}{N}}, m = -\frac{N}{2}, \cdots, \frac{N}{2} - 1 \quad (1)$$

where $X_i(n)$ denotes the M-QAM or M-PSK information symbol mapped on the nth sub-carrier of the ith OFDM symbol. The implementation is made easy by using an inverse fast Fourier transform (IFFT). To completely remove the inter symbol interference (ISI) in multi-path terrestrial systems, a guard interval is classically inserted between consecutive OFDM symbols. It usually consists of a copy at the beginning of each OFDM symbol of its last N_{CP} samples and is called cyclic prefix. In a fixed satellite broadcasting system, there is no ISI to cancel, but a cyclic prefix (CP) of limited length will be profitable for the coarse synchronization process [3]. At the output of the fixed satellite transmission channel, the received signal is corrupted by additive white gaussian noise of power spectral density $N_0/2$. In the receiver, the cyclic prefix is removed and a N bin FFT is applied to the sampled signal in order to recover the information transmitted on each sub-carrier. In absence of synchronization impairments, received symbols at the ith FFT output on subcarrier number n can be expressed as follows:

$$\widetilde{X}_i(n) = X_i(n) + w_i(n) \quad (2)$$

where $w_i(n)$ is a complex-valued gaussian noise sample.

B. Synchronization Impairments

In practise, synchronization impairments must be compensated in the receiver. They are described in this section, with their effects on the received symbols for an OFDM-based transmission over an AWGN channel.

B.1 Definition and Impact of the Clock Phase Error

The clock phase error is defined as the delay between the beginning T_0 of an OFDM symbols after CP removal and the first sampling instant T_0' in the receiver. After normalization to the OFDM symbol duration T, it is denoted as τ and is given by:

$$\tau = \frac{T_0 - T_0'}{T}. \quad (3)$$

Denoting T_{CP} the cyclic prefix length normalized to the OFDM symbol duration T, the condition $0 < \tau < T_{CP}$ guaranties the absence of inter symbol interference at the FFT output. In that case, a shift τ induces a simple phase rotation on each subcarrier [9]:

$$\widetilde{X}_i(n) = \exp(-j2\pi n\tau) X_i(n) + w_i(n). \quad (4)$$

If the first OFDM sample is outside the guard interval (i.e., if $\tau > T_{CP}$ or $\tau < 0$), inter symbol interferences appear, as well as inter carrier interferences (as the subcarrier orthogonality is lost), leading to the following expression for the received symbols [10]:

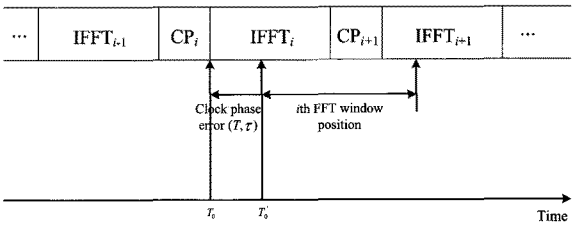

Fig. 1. Definition of the clock phase error.

$$\widetilde{X}_i(n) = (1 - |\alpha(\tau)|) \exp(-j2\pi n\tau) X_i(n) + I_\tau(n) + w_i(n) \quad (5)$$

where $\alpha(\tau) = \tau$ when the received signal is in advance with regard to the FFT window position ($\tau < 0$) and $\alpha(\tau) = \tau - T_{CP}$ when it is delayed with a delay exceeding the cyclic prefix duration ($\tau > T_{CP}$). $I_\tau(n)$ denotes the overall interference. Assimilating this interference to a gaussian additive noise [10] and assuming that the phase rotation induced by an error τ is corrected, the degradation on the bit error rate can be derived. This degradation is, for example, given on subcarrier number n for a M-QAM mapping, by the following expression:

$$D_n(\tau)_{\mathrm{dB}} = -20\log_{10} \frac{\left(1 - \alpha^2(\tau)\right)}{1 + \frac{P_n(\tau)}{N_0}} \quad (6)$$

where

$$P_n(\tau) = \alpha(\tau)^2 E_s \left[1 + 2 \sum_{k=-\frac{N}{2},\, k\neq n}^{\frac{N}{2}-1} \mathrm{sinc}^2[\pi(k-n)\alpha(\tau)]\right] \quad (7)$$

represents the power of $I_\tau(n)$ and E_s denotes the symbol energy.

B.2 Definition and Impact of the Clock Frequency Error

A sampling rate error arises from the difference between the received signal and the receiver sampling clock frequencies. It is defined after normalization as:

$$\beta = \frac{T_s' - T_s}{T_s} \quad (8)$$

where T_s and T_s' respectively stand for the received signal and the receiver sampling clock periods. The clock frequency error induces inter carrier interference. The received symbols become [9]

$$\widetilde{X}_i(n) = \mathrm{sinc}(n\beta)\, e^{j2\pi in\beta} X_i(n) + I_\beta(n) + w_i(n) \quad (9)$$

where $I_\beta(n)$ denotes the inter carrier interference due to an error β. It can be assimilated to an additive noise with power $P_n(\beta) = \frac{\pi^2}{3}(n\beta)^2$ [10].

B.3 Definition and Impact of the Carrier Frequency Error

The difference between the carrier frequency of the received signal and the receiver local oscillator frequency used for baseband translation is called carrier frequency error and will be denoted, after normalization to the subcarrier spacing Δf_p, as follows:

$$\Delta f = \frac{f_p' - f_p}{\Delta f_p} \tag{10}$$

where f_p represents the received signal carrier frequency and f_p' is the local oscillator frequency. A carrier frequency error breaks the orthogonality between the sub-carriers leading to inter carrier interference. The received symbols can be written as [11]:

$$\widetilde{X}_i(n) = e^{j\pi(2i+1)\Delta fT}\mathrm{sinc}(\pi\Delta fT)X_i(n) + I_{\Delta f}(n) + w_{i,n}. \tag{11}$$

$I_{\Delta f}(n)$ stands for the interference term due to Δf. Assimilating the interference to a gaussian noise and assuming that the phase rotation due to Δf is corrected, the degradation of the bit error rate can be derived. This degradation is for example given on subcarrier number n for a M-QAM mapping by:

$$D_n(\Delta f)_{\mathrm{dB}} = -20\log_{10}\frac{\mathrm{sinc}^2(\pi\Delta fT)}{1+\frac{P_n(\Delta f)}{N_0}} \tag{12}$$

where $P_n(\Delta f) = E_s\sum_{k=-\frac{N}{2}\ k\neq n}^{\frac{N}{2}-1}\mathrm{sinc}^2\left[\pi\left(\frac{k-n}{T}+\Delta f\right)T\right]$ represents the interference power.

B.4 Definition and Impact of the Carrier Phase Error

The carrier phase error stems from a difference between the received signal initial carrier phase and that of the local oscillator at the receiver. This carrier phase error, denoted as ϕ, does not introduce interference. In the presence of a phase shift ϕ, the received symbols can be written as:

$$\widetilde{X}_i(n) = e^{j\phi}X_i(n) + w_i(n). \tag{13}$$

The phase offset must be separately corrected at the receiver for each subcarrier of all OFDM symbols in order to correctly recover the transmitted information symbols: $X_i(n)$, $n = -N/2, \cdots, N/2-1$, $i = 0, 1, \cdots$

B.5 Overall Effect of Synchronization Impairments

The cumulated effects of all synchronization errors (τ, Δf, β and ϕ) are considered in the following expression of the received symbols:

$$\widetilde{X}_i(n) = Ae^{j\theta_i(n)}X_i(n) + I_i(n) + w_i(n) \tag{14}$$

where $I_i(n)$ denotes the overall interference term, A refers to the overall attenuation and $\theta_i(n)$ is the overall phase rotation. All these terms depend on τ, Δf, β and ϕ. Assuming that τ, Δf, β and ϕ are independent (this assumption has been assessed by simulations), $\theta_i(n)$ can be written as:

$$\theta_i(n) = \phi + 2\pi n\tau + \pi(2i+1)\Delta fT + 2\pi in\beta \tag{15}$$

III. PROPOSED RECEIVER

A receiver structure organized in three stages is proposed. It is represented on Fig. 2 and described below.

A. Correction of the clock phase and carrier frequency errors

In terrestrial radiocommunication systems, where the multipath channel is usually frequency selective, pilot aided algorithms are used in order to perform synchronization and channel estimation (see for example [12]–[14]). As channel estimation is not required for an AWGN channel, an attractive solution to perform synchronization without spectral efficiency loss is to use non data aided algorithms. A classical approach is to rely on the cyclic prefix [15]. As previously said, the introduction of a cyclic prefix is not required for multipath mitigation in a fixed satellite system. However, we propose to keep it with a limited length in order to aid a preliminary *coarse synchronization stage* in the receiver. Relying on this coarse synchronization, non data aided algorithms involving feedback propagation will track the residual timing and carrier frequency errors with better accuracy.

A.1 Coarse synchronization

The cyclic prefix, inserted at the beginning of each OFDM symbol, is a copy of its last N_{CP} samples. This redundancy is used to provide a first estimation of the symbol timing and carrier frequency [15]. In the case of a fixed satellite channel the likelihood function defined in [15] can be simplified as the channel is not frequency selective:

$$\widehat{T}_0 = \arg\max_k |R_L(k)|$$

$$\widehat{f}_p = -\frac{1}{2\pi}\arg\left[R_L(\widehat{T}_0)\right]$$

where

- $\widehat{T}_0$ is the estimate of the first sampling instant of the OFDM symbol (useful part),
- $R_L(k)$ represents the cross correlation function $R(k) = \sum_{l=0}^{N_{CP}-1} r^*(k+l)r(k+l+N)$ averaged on L consecutive OFDM symbols in order to improve the estimator performance. $r(k)$ denotes the kth received signal sample. However, the number of OFDM symbols in the averaging must be limited in order to reduce the interference caused by the clock frequency error.
- $\widehat{f}_p$ is the estimate of the received signal carrier frequency.

Note that with this method, the obtained estimate of the carrier frequency error presents an ambiguity. Indeed, this error is composed of an "integer part," i.e., a multiple of the subcarrier spacing, added to a fractional part of this spacing. However, only the second component can be recovered by the cross correlation estimation method. To estimate the "integer part" of the carrier frequency error, a pilot symbol is required [16]. Sub-carriers are retrieved without ambiguity at the FFT output by comparing the expected pilot with the corresponding received symbol.

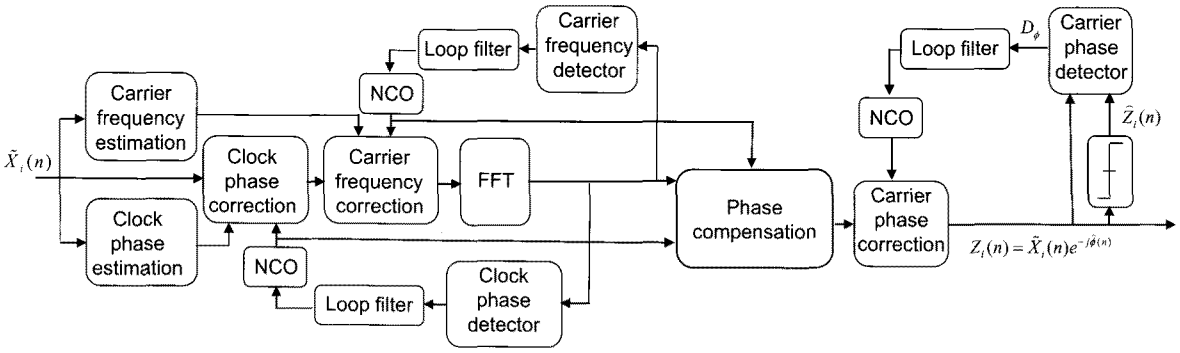

Fig. 2. Proposed receiver structure.

The normalized residual errors after coarse synchronization are:

$$\tau = \frac{\widehat{T}_0 - T_0}{T}$$

$$\Delta f = \frac{\widehat{f}_p - f_p}{\Delta f_p}$$

Their values must be within the acquisition range of the fine clock phase and carrier frequency loops which follow this preliminary stage. In this purpose, we have dimensioned the coarse synchronization in accordance with the fine synchronization algorithm requirements which actually depend on the loop parameters (see Section IV).

A.2 Fine Synchronization

The *fine synchronization stage* relies on two embedded loops based on phase measurements. The overall phase rotation $\theta_i(n)$ applied to the emitted symbols stems indeed from the synchronization errors Δf and τ (see (15)).

Carrier frequency detector

The set of phase errors affecting the symbols mapped on the subcarriers of two consecutive OFDM symbols, $\{\theta_i(n) - \theta_{i-1}(n)\}$, linearly depend on the subcarrier index n, with $\theta_i(0) - \theta_{i-1}(0) = 2\pi\Delta f$. The slope of this line, $2\pi\beta$, is very low compared to the value for $n = 0$ (see subsection II-B.2). Thus, Δf can be estimated by averaging $\{\theta_i(n) - \theta_{i-1}(n)\}$ on all subcarriers. Based on this observation, the carrier frequency detector can be written as:

$$D_{\Delta f}(i) = \arg\left[\sum_{n=-N/2}^{N/2-1}\left(\widetilde{X}_i(n)\widetilde{X}^*_{i-1}(n)\right)^4\right]. \quad (16)$$

The elevation to the power 4 allows to remove the modulation assuming M-QAM mapping on all subcarriers with $M \geq 4$).

Clock phase detector

For a given OFDM symbol index i and for $\beta << \tau$, the set of phase errors $\{\theta_i(n)\}_{n=-\frac{N}{2},\cdots,\frac{N}{2}-1}$ defines a line, the slope of which is proportional to τ. As a consequence, the clock phase detector can be written as [17]:

$$D_\tau(i) = \arg\left[\sum_{n=-N/2}^{N/2-1}\left(\widetilde{X}_i(n+1)\widetilde{X}^*_i(n)\right)^4\right]. \quad (17)$$

In order to improve the performance of the detector, a pre-summation on w consecutive symbols is performed:

$$D_\tau(i) = \arg\left[\sum_{p=2}^{N/w} Q_p Q^*_{p-1}\right], \quad (18)$$

with

$$Q_p = \frac{1}{w}\sum_{n=0}^{w-1}\widetilde{X}^4_i(n - \frac{N}{2} + pw). \quad (19)$$

Parameter w can be adjusted. The detector performance increases with w because the pre-summation allows to improve the signal to noise ratio. On the other hand, increasing w leads to shorter the loop acquisition range, which requires better performance for the coarse synchronization process.

B. Correction of the Sampling Clock Frequency Error

In the considered satellite systems, the sampling clock frequency error β is very low compared to the sampling rate. Indeed, the receiver sampling clocks are generally more stable in a satellite transmission than in terrestrial systems. Common values for the normalized error β are between 10^{-4} and 10^{-5} leading to very low values for $P_n(\beta)$ (see subsection II-B.2) and negligible degradation. For that reason, there is no requirement for a specific synchronization block to correct the sampling clock frequency error. Nevertheless, it must be taken into account in the synchronization structure because it leads to a long term drift of the sampling instants.

C. Correction of the Carrier Phase Error

In the considered context (fixed satellite transmissions), the channel is not frequency selective. As a consequence, channel equalization is not performed at the receiver (contrarily to terrestrial systems). Consequently, after coarse and fine synchronization, a residual carrier phase error remains to be corrected

on all sub-carriers. Moreover, the impact of previous synchronization stages on the carrier phase must be taken into account. Indeed, the residual clock phase error involves a phase rotation on each subcarrier. Its correction being quantified (K samples each N_K OFDM symbols), it induces phase "jumps." Moreover, the residual carrier frequency error generates a very penalizing phase noise on each subcarrier.

We have used the carrier phase detector proposed in [18]:

$$D_\phi = \operatorname{sgn}\left(\operatorname{Im}\left[Z_i(n)\right]\right)\left(\operatorname{Re}\left[\widehat{Z}_i(n)\right] - \operatorname{Re}\left[Z_i(n)\right]\right) - \operatorname{sgn}\left(\operatorname{Re}\left[Z_i(n)\right]\right)\left(\operatorname{Im}\left[\widehat{Z}_i(n)\right] - \operatorname{Im}\left[Z_i(n)\right]\right), \quad (20)$$

where

- $Z_i(n) = \widetilde{X}_i(n)e^{-j\widehat{\phi}(n)}$, $\widehat{\phi}(n)$ being the estimated carrier phase on subcarrier number n.
- $\widehat{Z}_i(n)$ is the decided symbol from $Z_i(n)$.
- $\operatorname{Re}[\cdot]$ and $\operatorname{Im}[\cdot]$ stand for real and imaginary parts, and $\operatorname{sgn}(\cdot)$ for the sign function, respectively.

In order to take into account the impact of the previous synchronization stages, the proposed receiver includes a phase compensation block (see Fig. 2). Indeed, the phase rotation introduced by the residual clock phase error, as well as the one associated to the residual carrier frequency error, are known and can be compensated.

IV. PERFORMANCE

A. Fine Synchronization

A.1 Clock Phase Loop

The theoretical standard deviation of the residual clock phase error at the output of the clock phase loop is a function of the loop bandwidth (B_lT), the symbol to noise ratio (E_s/N_0), the number of subcarriers (N) and the parameter w [19]:

$$\sigma_\tau \simeq \frac{N^2 B_l T}{32\pi^2(N-w)w(E_s/N_0)} \cdot \left[2 + \frac{9}{E_s/N_0} + \frac{12}{(E_s/N_0)^2} + \frac{3}{(E_s/N_0)^3}\right] \cdot \left[19 + \frac{244}{E_s/N_0} + \frac{966}{(E_s/N_0)^2} + \frac{1068}{(E_s/N_0)^3} + \frac{267}{(E_s/N_0)^4}\right]. \quad (21)$$

As expected, the performance of the clock phase loop increases with w. However, at the same time, the loop acquisition range becomes shorter. The clock phase loop can tolerate some ISI coming from the previous coarse synchronization stage. Thus, its acquisition range can exceed the cyclic prefix duration T_{CP}. Fig. 3 plots, as a function of w, the tolerated clock phase loop acquisition range exceeding T_{CP}. QPSK and 16-QAM mapping have been considered on each subcarrier, as well as several values of N. Reducing the loop acquisition range will impose better performance to the coarse synchronization process, requiring a longer cyclic prefix and leading to reduce spectral efficiency. Thus, a trade off has to be found on the value of w. Fig. 3 also shows that the clock phase loop acquisition range does not depend, neither on the carried modulation, nor on the number of sub-carriers. It also does not depend on E_b/N_0 ratio (see Fig. 4). Fig. 5 shows the standard deviation of the residual clock phase error, σ_τ, plotted as a function of E_b/N_0. A plateau appears for high values of E_b/N_0. This is due to the fact that the clock phase error correction is not continuous, as the minimum step corresponds to the duration of one sample of the OFDM symbol, leading to a uniform quantization noise with standard deviation $1/2\sqrt{3}N$. On Fig. 5, $N = 512$, leading to a plateau for $\sigma \simeq 5.6 \times 10^{-4}$. As illustrated, this plateau can be limited through oversampling which removes the quantization effect.

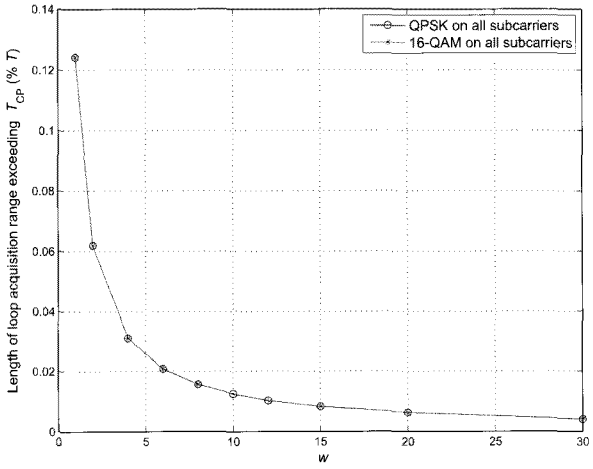

Fig. 3. Clock phase loop acquisition range depending on parameter w.

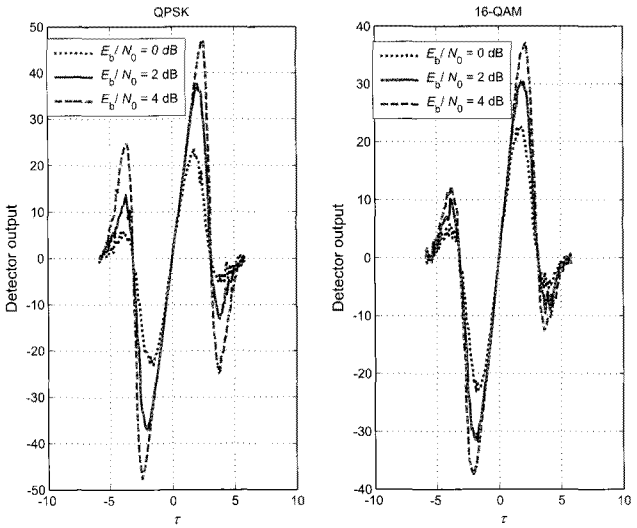

Fig. 4. S-curves of clock phase loop detector.

A.2 Carrier Frequency Loop

The theoretical standard deviation of the residual carrier frequency error at the output of the carrier frequency loop is a function of the loop bandwidth (B_lT), the symbol to noise ratio

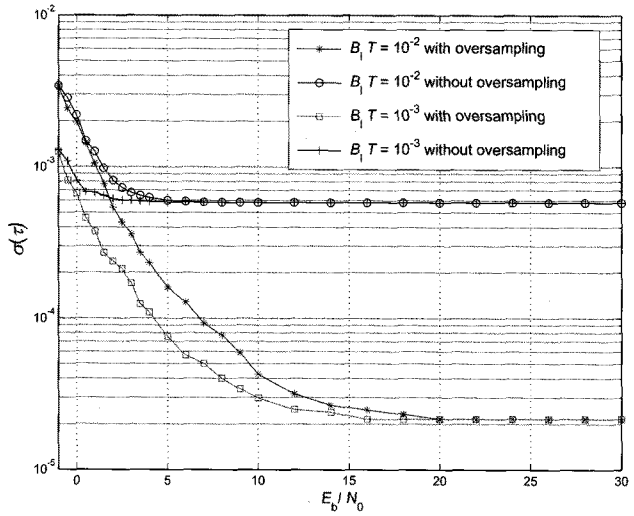

Fig. 5. Performance of fine symbol timing synchronization with oversampling operation.

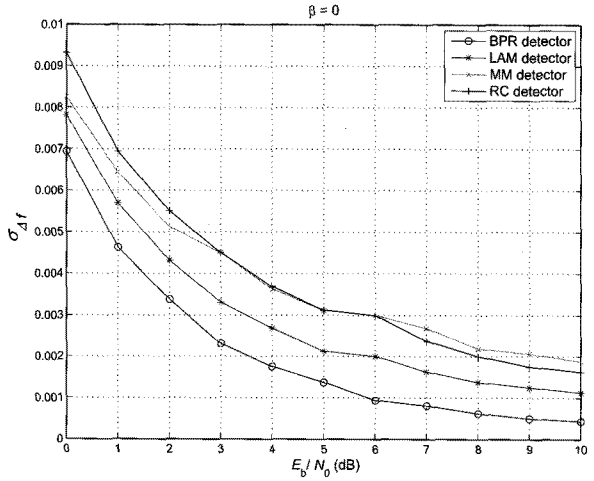

Fig. 6. Performance of fine carrier frequency synchronization without clock frequency error ($\beta = 0$).

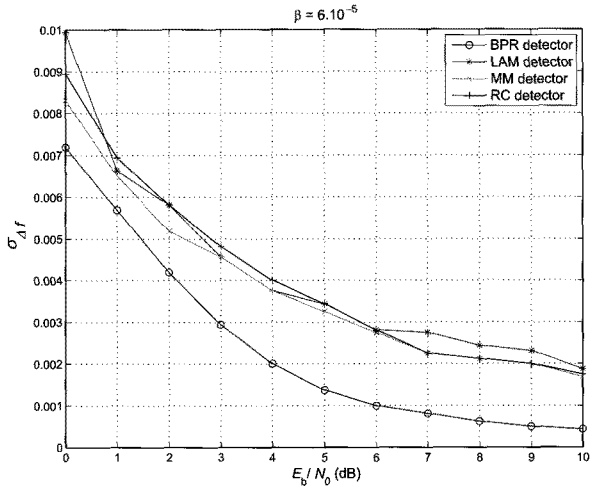

Fig. 7. Performance of fine carrier frequency synchronization in presence of a clock frequency error ($\beta = 6 \cdot 10^{-5}$).

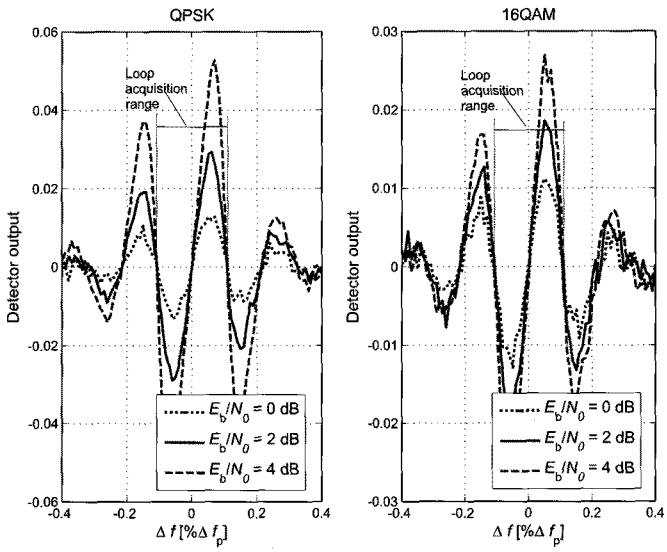

Fig. 8. S-curve of carrier frequency detector.

(E_s/N_0) and the number of sub-carriers (N). It is given by [19]:

$$\sigma_{\Delta_f} \simeq \frac{B_l T}{32\pi^2 N(E_s/N_0)} \cdot \left[2 + \frac{9}{E_s/N_0} + \frac{12}{(E_s/N_0)^2} + \frac{3}{(E_s/N_0)^3}\right] \cdot \left[19 + \frac{244}{E_s/N_0} + \frac{966}{(E_s/N_0)^2} + \frac{1068}{(E_s/N_0)^3} + \frac{267}{(E_s/N_0)^4}\right].$$

The performance of the proposed carrier frequency detector (labeled BPR: Based on phase rotation) is compared on Figs. 6 and 7 with several detectors proposed in the literature and respectively labeled LAM [6] , RC [7], and MM [20] (from their author initials). For both figures $N = 512$, $B_l T = 10^{-2}$ and QPSK mapping are assumed. Fig. 6 considers $\beta = 0$, while Fig. 7 considers $\beta = 6 \cdot 10^{-5}$. The proposed detector outperforms the other ones, especially in the presence of a clock frequency error ($\beta \neq 0$). It can be noted that the negligible degradation on the performance due to the clock frequency error justifies the absence of a dedicated correction structure for β.

Fig. 8 illustrates the S-curve of the carrier frequency detector for several values of E_b/N_0 and for QPSK and 16-QAM carried modulations. It shows that the carrier frequency loop acquisition range $[-\Delta f_{\max}\ \Delta f_{\max}]$ does not depend neither on the carried modulation nor on E_b/N_0. Fig. 9 plots $\Delta f_{\max}$ as a function of the number of subcarriers N for QPSK and 16-QAM mapping. It shows that its value is the same and equals $11.5\%\Delta f_p$ whatever N and the mapping may be.

B. Coarse Synchronization

The cyclic prefix is used to provide a first estimate of the clock phase and the carrier frequency of the received signal. The residual estimation errors have to fit with the fine synchronization loop acquisition ranges, i.e.:

- $[-\Delta f_{\max}\ \Delta f_{\max}]$, with $\Delta f_{\max} = 11.5\%\Delta f_p$ for the carrier

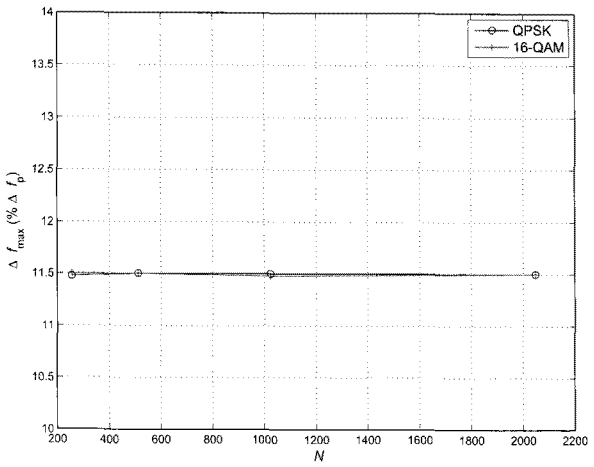

Fig. 9. Carrier frequency loop acquisition range $[-\Delta f_{\max} \Delta f_{\max}]$ is independent of N.

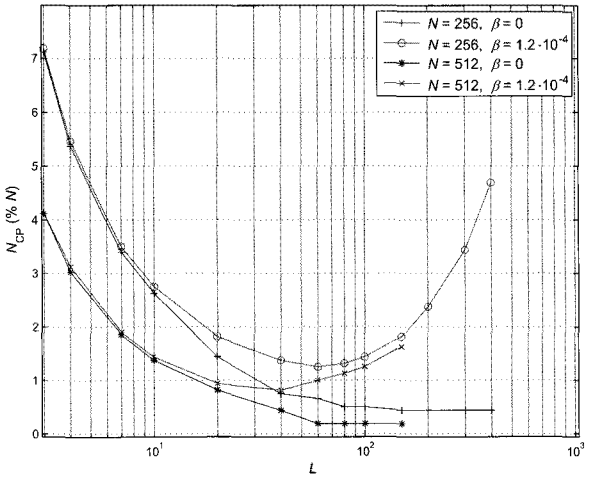

Fig. 10. Required cyclic prefix length to ensure a probability lower than 10^{-6} for the residual clock phase error to exceed the acquisition range.

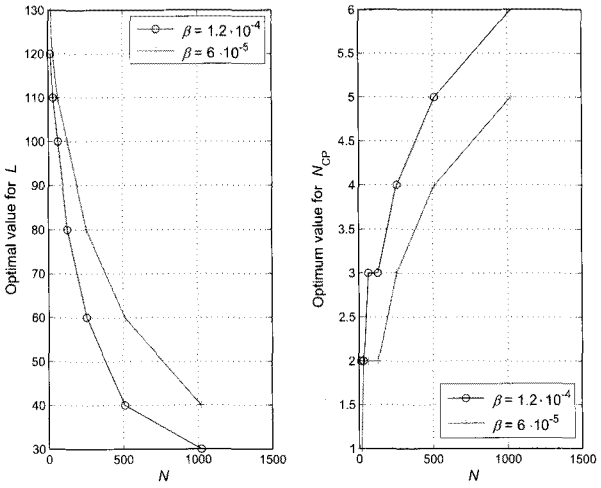

Fig. 11. Optimal values for parameters L and N_{CP}

frequency loop.

- depending on w for the clock phase loop.

In order to maximize the spectral efficiency, the size of the cyclic prefix has to be minimized. This size (N_{CP} samples) depends on the number L of OFDM symbols on which the cross correlation is averaged. In absence of clock frequency error ($\beta = 0$), increasing L allows to improve the estimator performance and allows to reduce the cyclic prefix length. But when $\beta \neq 0$ the increase of L induces ISI which degrades the estimator performance. As a compensation it is necessary to increase the cyclic prefix length. Fig. 10 plots the needed cyclic prefix size (N_{CP} samples) as a function of L to guarantee a probability lower than 10^{-6} to have the residual clock phase error exceed the acquisition range. Two values of N have been considered, parameter w has been set to 4 and $E_b/N_0 = 0$ dB. The symbol mapping has no influence since the estimation is performed before the FFT. It can be observed that, in the presence of a clock frequency error β, an optimal value (leading to a minimum length for the cyclic prefix) exists for parameter L. This optimal value depends on N, β and w. Fig. 11 shows the optimal values of L and N_{CP} as a function of N for $\beta = 1.2 \cdot 10^{-4}$ and $\beta = 6 \cdot 10^{-4}$ (w being set to 4).

C. Carrier Phase Synchronization

C.1 Impact of Previous Synchronization Stages

The residual clock phase error induces a phase rotation on each subcarrier. The correction coefficient is updated each N_K OFDM symbols. This introduces phase jumps on each subcarrier. As a response to phase jumps an additional phase compensation block is introduced (see Fig. 2). Fig. 12 shows the carrier phase evolution before and after this compensation as a function of the OFDM symbol index. The considered subcarrier is $n = 108$, the clock frequency error is $\beta = 6 \cdot 10^{-5}$, the number of sub-carriers $N = 256$ and the correction is done each $N_K = 60$ OFDM symbols. We observe that phase jumps (about 150 degrees) are efficiently removed by the phase compensation block. The residual carrier frequency error generates a phase noise on each subcarrier at the input of the carrier phase loop. Fig. 13 plots the standard deviation of the residual carrier phase error, averaged on $N = 256$ QPSK modulated subcarriers, as a function of the carrier phase loop noise bandwidth $B_l T$. The carrier frequency loop noise bandwidth (normalized to the OFDM symbol rate) has been set to 10^{-3} and $E_b/N_0 = 5$ dB. As expected, we can observe the classical trade-off to be performed on $B_l T$ value, but the phase noise due to the residual carrier frequency error is very penalizing. To avoid it, the phase rotation induced by the residual carrier frequency error is compensated at the carrier phase loop input. The obtained standard deviation for the residual carrier phase error then classically increases with thermal noise.

C.2 Impact of Phase Noise

Three models are considered for the phase noise: two models compliant with the templates respectively provided in DVB-S2 and DVB-SH standards [2], [8], and a Wiener phase noise model [21]. In order to limit the degradation on the BER to 0.2 dB at the DVB-S2 standard decoder output, it is shown in

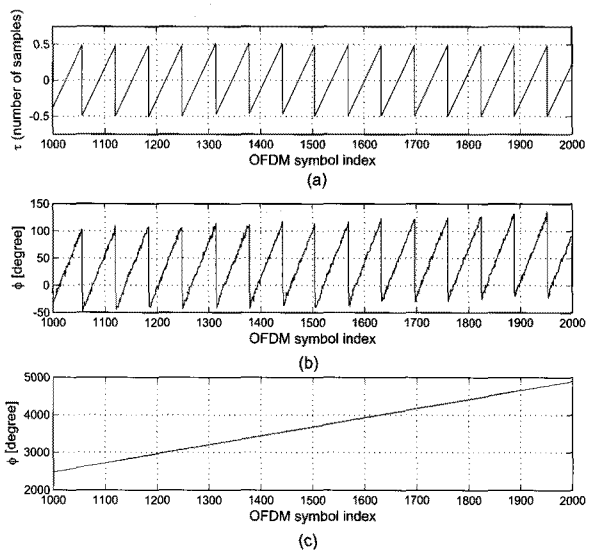

Fig. 12. Effect of the phase compensation block on the carrier phase evolution: (a) Residual clock phase evolution [samples], (b) carrier phase before compensation, and (c) carrier phase after compensation.

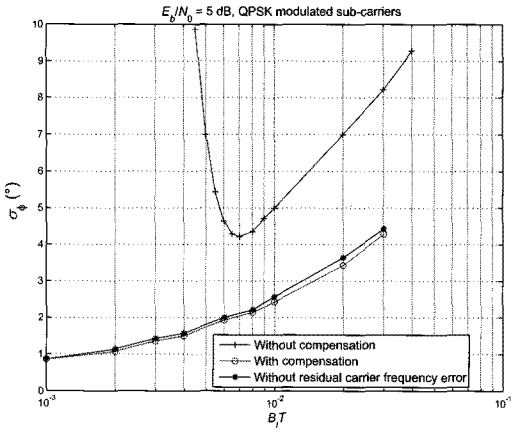

Fig. 13. Standard deviation of the residual carrier phase error.

[22] that the standard deviation for the residual carrier phase error has to be lower than 8° for QPSK modulation. Considering QPSK modulated sub-carriers, Fig. 14 plots the standard deviation of the residual carrier phase error σ_ϕ as a function of the loop bandwidth B_lT in the presence of a "DVB-S2 compliant" phase noise but with no thermal noise. For $B_lT < 10^{-2}$ (necessary condition for the loop to converge at $E_b/N_0 = 0$ dB), $\sigma_\phi > 10.5°$. The proposed receiver is not likely to be able to cope with such phase noise. This can be explained by the fact that phase noise is N times faster on each sub-carrier (when compared to the symbol rate) than in a single carrier transmission. Fig. 15 plots the residual carrier phase error σ_ϕ as a function of the loop bandwidth B_lT in the presence of a "DVB-SH compliant" standard phase noise. Several values are considered for E_b/N_0, $N = 256$ and a QPSK mapping is assumed on each subcarrier. The classical trade-off on the loop bandwidth to minimize the residual carrier phase error standard deviation is performed. Fig. 16 shows the standard deviation of the residual

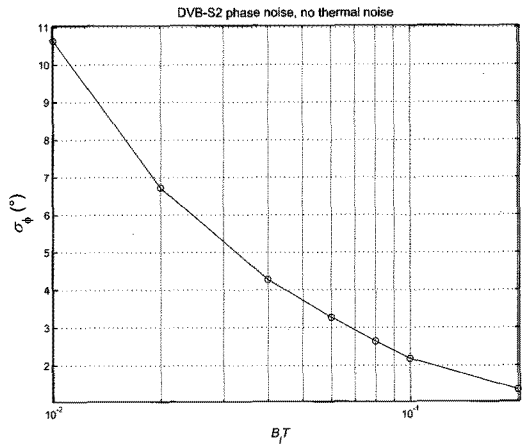

Fig. 14. Standard deviation of the residual carrier phase error in the presence of "DVB-S2 compliant" phase noise.

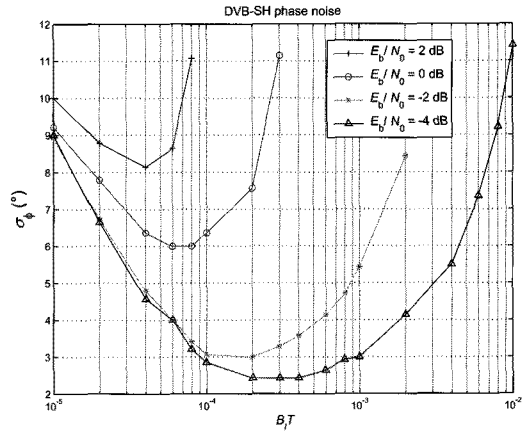

Fig. 15. Standard deviation of the residual carrier phase error in the presence of "DVB-SH compliant" phase noise.

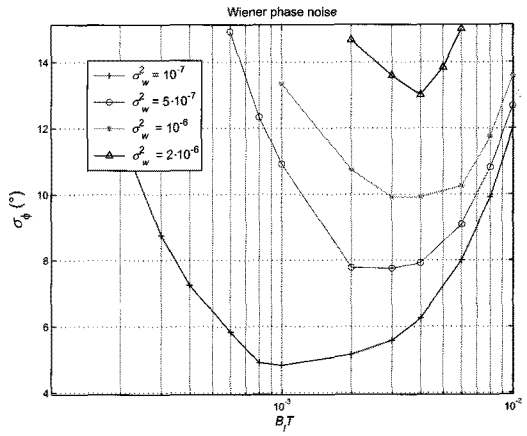

Fig. 16. Standard deviation of the residual carrier phase error in the presence of Wiener phase noise.

carrier phase error σ_ϕ as a function of the loop bandwidth B_lT with a Wiener phase noise model. Several values are considered for the Wiener phase noise power (σ_w^2), sub-carriers are QPSK modulated, $N = 256$ and $E_b/N_0 = 0$ dB.

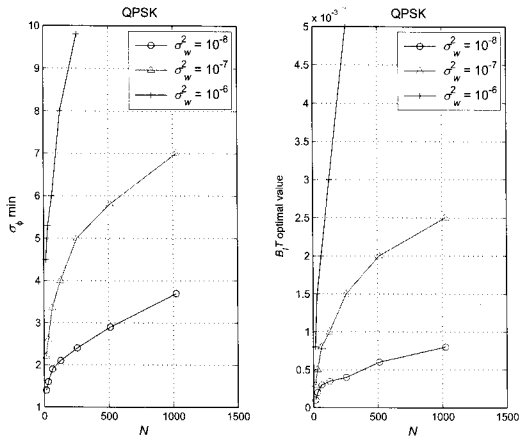

Fig. 17. σ_ϕ min and B_lT optimal value, in the presence of Wiener phase noise, for QPSK mapping.

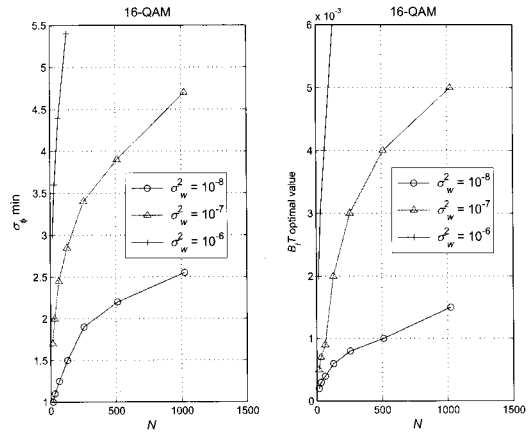

Fig. 18. σ_ϕ min and B_lT optimal value, in the presence of Wiener phase noise, for 16-QAM mapping.

	$E_b/N_0 = 0$ dB		$E_b/N_0 = -1$ dB		$E_b/N_0 = -2$ dB	
N	σ_w max	B_lTopt	σ_w max	B_lTopt	σ_w max	B_lTopt
16	$9.4\ 10^{-6}$	$2.8\ 10^{-3}$	$5.1\ 10^{-6}$	$1.2\ 10^{-3}$	$2\ 10^{-6}$	$9\ 10^{-4}$
32	$4.2\ 10^{-6}$	$2.7\ 10^{-3}$	$2.8\ 10^{-6}$	$1.6\ 10^{-3}$	$9\ 10^{-7}$	$1.2\ 10^{-3}$
64	$2\ 10^{-6}$	$3\ 10^{-3}$	$1.2\ 10^{-6}$	$1.5\ 10^{-3}$	$6\ 10^{-7}$	10^{-3}
128	$1.1\ 10^{-6}$	$2.8\ 10^{-3}$	$7\ 10^{-7}$	$1.6\ 10^{-3}$	$3.5\ 10^{-7}$	$9.5\ 10^{-4}$
256	$6\ 10^{-7}$	$3\ 10^{-3}$	$3.5\ 10^{-7}$	$1.5\ 10^{-3}$	$1.5\ 10^{-7}$	$8\ 10^{-4}$
512	$2.8\ 10^{-7}$	$3.2\ 10^{-3}$	$1.4\ 10^{-7}$	$1.4\ 10^{-3}$	$7\ 10^{-8}$	$9\ 10^{-4}$
1024	$1.2\ 10^{-7}$	$2.9\ 10^{-3}$	$8\ 10^{-8}$	$1.3\ 10^{-3}$	$4\ 10^{-8}$	$8\ 10^{-4}$

Table 1. Wiener noise maximal power value and optimal B_lT value - QPSK mapping

	$E_b/N_0 = 0$ dB		$E_b/N_0 = -1$ dB		$E_b/N_0 = -2$ dB	
N	σ_w max	B_lTopt	σ_w max	B_lTopt	σ_w max	B_lTopt
16	$5.6\ 10^{-7}$	$1.5\ 10^{-3}$	$3.1\ 10^{-7}$	$8.2\ 10^{-4}$	$2.1\ 10^{-7}$	$5.9\ 10^{-4}$
32	$2.9\ 10^{-7}$	$1.2\ 10^{-3}$	$1.7\ 10^{-7}$	$7.5\ 10^{-4}$	10^{-7}	$6.1\ 10^{-4}$
64	$1.6\ 10^{-7}$	10^{-3}	10^{-7}	$8.1\ 10^{-4}$	$7\ 10^{-8}$	$6.7\ 10^{-4}$
128	$6.5\ 10^{-8}$	$1.3\ 10^{-3}$	$7\ 10^{-7}$	$8.4\ 10^{-4}$	$3.3\ 10^{-8}$	$6.4\ 10^{-4}$
256	$3.2\ 10^{-8}$	$1.4\ 10^{-3}$	$3.5\ 10^{-7}$	$7.9\ 10^{-4}$	$1.5\ 10^{-8}$	$6\ 10^{-4}$
512	$1.8\ 10^{-8}$	$1.2\ 10^{-3}$	$1.3\ 10^{-8}$	$8.5\ 10^{-4}$	$9.5\ 10^{-9}$	$5.5\ 10^{-4}$
1024	$9\ 10^{-9}$	$1.1\ 10^{-3}$	$6.1\ 10^{-9}$	$8\ 10^{-4}$	$3.5\ 10^{-9}$	$5\ 10^{-4}$

Table 2. Wiener noise maximal power value and optimal B_lT value - 16-QAM mapping.

D. Performance Assessment of the Proposed Receiver

The global performance of the overall structure is studied in the presence of "Wiener" or "DVB-SH compliant" phase noise, as a function of the carrier phase loop bandwidth B_lT, E_b/N_0 and the number N of sub-carriers.

D.1 In the Presence of Wiener Phase Noise

For $E_b/N_0 = 0$ dB and QPSK modulated sub-carriers, Fig. 17 plots the minimum value of the standard deviation of the residual carrier phase error (denoted as σ_ϕ min) and the optimal value of B_lT, both as a function of N and for several values of the Wiener phase noise power σ_w^2. The same parameters are plotted on Fig. 18 for $E_b/N_0 = 4$ dB and 16-QAM modulated sub-carriers. For each value of E_b/N_0 and N, the maximum acceptable power of "Wiener" phase noise, as well as the optimal value of B_lT, can be deducted from simulations to minimize the standard deviation of the residual carrier phase error. They are given in table 1 for QPSK modulation in order to obtain $\sigma_{phi} < 8°$ (leading to a limited degradation on the BER of 0.2 dB at the DVB-S2 standard output decoder) and in table 2 for 16-QAM modulation in order to obtain $\sigma_{phi} < 2.6°$ (also leading to a limited degradation on the BER to 0.2 dB at the DVB-S2 standard output decoder).

D.2 In the Presence of DVB-SH Phase Noise

Fig. 19 (QPSK modulated sub-carriers) and Fig. 20 (16QAM modulated sub-carriers) plot the minimum value of the standard deviation of the residual carrier phase error (denoted σ_ϕ min) and the optimal value of B_lT, both as a function of N and for several values for E_b/N_0. For each value of N, table 3 gives the minimum required E_b/N_0 ratio and the corresponding optimal loop bandwidth B_lT in order to obtain a standard deviation of the residual carrier phase error lower than $8°$ (QPSK) or $2.6°$ (16-QAM).

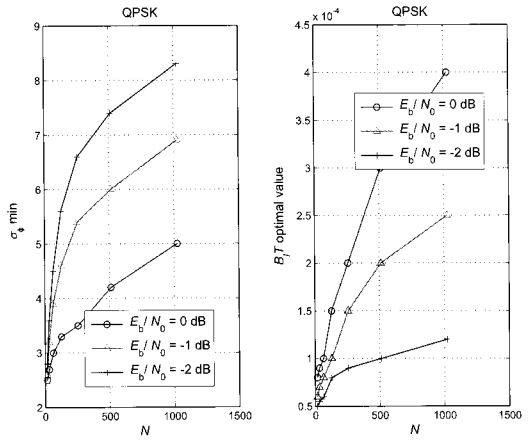

Fig. 19. σ_ϕ min and B_lT optimal value, in the presence of "DVB-SH compliant" phase noise, for QPSK mapping.

D.3 Spectral efficiency

We finally compare in this section the proposed transmission scheme with a DVB-S2 standard solution for broadband satellite applications, in terms of spectral efficiency. No comparison is provided here with the DVB-SH OFDM waveform, as it is not suited to the considered broadband satellite communication

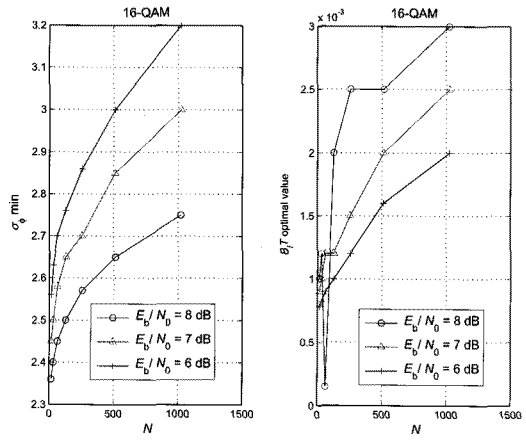

Fig. 20. σ_ϕ min and B_lT optimal value, in the presence of "DVB-SH compliant" phase noise, for 16-QAM mapping.

	QPSK		16-QAM	
N	E_b/N_0 min (dB)	B_lTopt	E_b/N_0 min (dB)	B_lTopt
16	-4.1	$2.5\ 10^{-5}$	5.7	$7.5\ 10^{-4}$
32	-3.8	$3\ 10^{-5}$	6.2	$8.5\ 10^{-4}$
64	-3.6	$3.8\ 10^{-5}$	6.8	10^{-3}
128	-3.3	$4.8\ 10^{-5}$	7.3	$1.5\ 10^{-3}$
256	-3	$6\ 10^{-5}$	7.8	$2\ 10^{-3}$
512	-2.3	$9\ 10^{-5}$	8.2	$2.5\ 10^{-3}$
1024	-1.8	$1.5\ 10^{-4}$	8.5	$3.2\ 10^{-3}$

Table 3. E_b/N_0 required minimum value and optimal B_lT value to obtain $\sigma_\phi < 8°$ for QPSK mapping and $\sigma_\phi < 2.68°$ for 16-QAM mapping.

context.

Depending on the loop parameters, the required cyclic prefix length, $N_{CP_{\min}}$, can be computed. The bandwidth occupied by the OFDM signal depends on $N_{CP_{\min}}$ and on the number of side lobes considered on the OFDM signal power spectral density. Assuming that two lobes are considered, B_{MC} can be written as:

$$B_{MC} = \left(1 + \frac{N_{CP_{\min}}}{N}\right)\left(1 + \frac{5}{N}\right) R_s. \tag{22}$$

For the same useful symbol rate R_s, the required bandwidth B_{MC} can be compared to that of a single carrier raised cosine waveform :

$$B_{SC} = (1 + \alpha)R_s \tag{23}$$

where α denotes the roll-off factor. We define the gain on the spectral efficiency by the following:

$$G = \frac{B_{SC} - B_{MC}}{B_{SC}}. \tag{24}$$

It is provided in table 4 considering both roll-off factors proposed in DVB-S2 standard: $\alpha = 0.35$ and $\alpha = 0.2$. Using proposed OFDM waveform yields to a shorter bandwidth from $N = 32$ for $\alpha = 0.35$ and from $N = 64$ for $\alpha = 0.2$.

V. CONCLUSIONS

This paper addresses the performance of an OFDM transceiver to be used over a fixed satellite channel. The motivation for using OFDM in such context is to improve the spectral

	$\alpha = 0.35$		$\alpha = 0.2$	
N	$\beta = 1.2 \cdot 10^{-4}$	$\beta = 6 \cdot 10^{-5}$	$\beta = 1.2 \cdot 10^{-4}$	$\beta = 6 \cdot 10^{-5}$
16	−9.8%	−3.3%	−23.1%	−16.2%
32	9%	9%	−2.4%	−2.4%
64	16.4%	17.6%	5.9%	7.6%
128	21.2%	21.8%	11.4%	12.1%
256	23.3%	23.6%	13.7%	14%
512	24.5%	24.6%	15%	15.2%
1024	25.1%	25.2%	15.8%	15.9%

Table 4. Bandwidth reduction for the proposed transceiver compared to a DVB-S2 transmission

efficiency with regard to existing single carrier fixed broadband systems. Indeed, contrarily to OFDM-based terrestrial systems, the overhead induced by pilot symbols and guard intervals can be reduced to the minimum in such context. There is no ISI to cancel (no multi-path) and no need for channel equalization. The only part of the overhead still needed is for synchronization purposes. The proposed receiver relies on a short cyclic prefix to perform a first coarse synchronization. Relying on this coarse synchronization, a fine synchronization based on non pilot aided loop structures is defined. Both processes are optimized to minimize the required overhead. Our simulations show the good performance of the proposed receiver. Moreover, the cyclic prefix length reduction allows to shorter the occupied bandwidth in comparison with single carrier fixed broadband systems with DVB-S2 waveform.

REFERENCES

[1] "Digital video broadcasting (DVB): Framing structure, channel coding and modulation for 11/12 GHz satellite services–Ref. ETSI EN 300 421 v1.1.2," Aug. 1997.

[2] "Digital Video Broadcasting (DVB): User guiderlines for the second generation system for broadcasting, interactive services, news gathering and other broadband satellite applications (DVB-S2)–Ref. ETSI TR 102 376 v1.1.1," Feb. 2005.

[3] M. Morelli, C.-C. J. Kuo, and M.-O. Pun, "Synchronization techniques for orthogonal frequency division multiple access (OFDMA): A tutorial review," *Proc. IEEE*, vol. 95, no. 7, pp. 1394–1427, July 2007.

[4] B. Ai, Z.-X. Yang, C.-Y. Pan, J.-H. Ge, and Y. W. Z. Lu, "On the synchronization techniques for wireless OFDM systems," *IEEE Trans. Broadcast.*, vol. 52, no. 2, pp. 236–244, June 2006.

[5] S. A. Fechtel, "OFDM carrier and sampling frequency synchronization and its performance on stationary and mobile channels," *IEEE Trans. Consum. Electron.*, vol. 46, no. 3, pp. 438–441, Aug. 2000.

[6] V. Lottici, A. N. D'Andrea, and U. Mengali, "A new frequency loop for OFDM systems," *IEEE Trans. Consum. Electron.*, vol. 46, no. 4, pp. 970–979, Nov. 2000.

[7] H. Roh and K. Cheun, "Non-data-aided spectral-line method for fine carrier frequency synchronization in OFDM receivers," *JCN*, vol. 6, no. 2, June 2004.

[8] "Digital video broadcasting (DVB); Framing structure, channel coding, and modulation for satellite services to handheld devices (SH) below 3 GHz–Ref. ETSI EN 302 583 v1.1.0," Jan. 2008

[9] B. Yang, K. B. Letaief, R. S. Cheng, and Z. Cao, "Timing recovery for OFDM transmission," *IEEE J. Sel. Areas Commun.*, vol. 18, no. 11, pp. 2278–2291, Nov. 2000.

[10] M. Speth, S. A. Fechtel, G. Fock, and H. Meyr, "Optimum receiver design for wireless broad-band systems using OFDM-Part 1," *IEEE Trans. Commun.*, vol. 47, no. 11, pp. 1668–1677, Nov. 1999.

[11] T. Pollet, M. Van Bladel, and M. Moeneclaey, "BER sensitivity of OFDM systems to carrier frequency offset and Wiener phase noise," *IEEE Trans. Commun.*, vol. 43, pp. 191–193, 1995.

[12] S.-H. Chen, W.-H. He, H.-S. Chen, and Y. Lee., "Mode detection, synchronization and channel estimation for DVB-T OFDM receiver," in *Proc. IEEE GLOBECOM*, vol. 5, San Francisco, USA, Dec. 2003, pp. 2416–2420.

[13] E. G. Larsson, L. Guoqing, L. Jian, and G. B. Giannakis, "Joint symbol timing and channel estimation for OFDM based WLANs," *IEEE Commun. Lett.*, vol. 5, no. 8, pp. 325–327, Aug. 2001.

[14] H.-K. Song, Y.-H. You, J.-H. Paik, and Y.-S. Cho, "Frequency-offset synchronization and Channel estimation for OFDM-based transmission," *IEEE Commun. Lett.*, vol. 4, no. 3, pp. 95–97, Mar. 2000.
[15] J. J. Van de Beek, M. Sandelland, and P. O. Borjesson, "ML estimation of time and frequency offset in OFDM systems," *IEEE Trans. Signal Process.*, vol. 45, no. 7, pp. 1800–1805, July 1997.
[16] M. Schmidl and D. C. Cox, "Robust frequency and timing synchronization for OFDM," *IEEE Trans. Commun.*, vol. 45, no. 12, pp. 1613–1621, Dec. 1997.
[17] D. Lee and K. Cheun, "A new symbol timing recovery algorithm for OFDM systems," *IEEE Trans. Consum. Electron.*, vol. 43, no. 3, pp. 767–775, June 1997.
[18] A. Metref, D. Le Guennec, and J. Palicot, "Optimized Decision-Directed Carrier Recovery Loop for 16-QAM Constellations," in *Proc. IEEE GLOBECOM*, Washington, USA, Nov. 2007, pp. 3112–3117.
[19] A. T. Ho, "Application des techniques multiporteuses de type OFDM pour les futurs systèmes de télécommunications par satellite," Ph.D. dissertation, Institut National Polytechnique de Toulouse, 2009.
[20] M. Morelli and U. Mengali, "An improved frequency offset estimator for OFDM applications," *IEEE Commun. Lett.*, vol. 3, no. 3, pp. 75–77, Mar. 1999.
[21] A. Papoulis, *Probability, Random Variables and Stochastic Processes*, McGraw-Hill, 1965.
[22] A. Ginesti, *Process for Pilot Aided Carrier Phase Synchronization*, Rapport technique ESA, Sept. 2003.

Nathalie Thomas was born in Versailles, France, in 1967. She received the Eng. degree in Electrical Engineering from the Ecole Nationale Supérieure d'Electrotechnique, Electronique, Informatique et Télécommunications (ENSEEIHT), in Toulouse, France, in June 1991. The same year she received the M.Sc. degree in Signal and Image Processing from the National Polytechnic Institute of Toulouse and, in January 1995, the Ph.D. degree in Signal and Image Processing. Since 1995 she has been an Assistant Professor and works with the National Polytechnic Institute, University of Toulouse, since 2000. She belongs to the Signal and Communication Group of the IRIT Laboratory and her major research interest is in advanced digital communication techniques.

Marie-Laure Boucheret received the Eng. degree in Electrical Engineering from ENST Bretagne, Rennes, France, and the M.Sc. degree in Signal Processing from the University of Rennes, both in June 1985. In june 1997, she received the Ph.D. degree in Communications from TELECOM ParisTech, and the "Habilitation à diriger les recherches" in June 1999 from INPT University of Toulouse. From 1985 to 1986 she has been a research Engineer at the French Philips Research Laboratory (LEP). From 1986 to 1991, she has been an engineer at Thales Alenia Space, first as a project Engineer (TELECOM II program) then as a Study Engineer at the Transmission Laboratory. From 1991 to 205 she was a Associated professor then a Professor at TELECOM ParisTech. Since March 2005 Marie-Laure Boucheret is a Professor at the National Polytechnic Institute of Toulouse (ENSEEIHT - University of Toulouse). She is also with the Signal and Communication group of the IRIT Laboratory.

Anh Tai Ho was born was born in Ha Tinh, Vietnam, on May 2, 1982. He received the Eng. degree in Electronics and Communication Systems and the M.Sc. degree in Micro-Electronics, Architecture, Networks and Systems from National Institute of Applied Sciences of Rennes, France, both in July 2005. He received his Ph.D. degree from the National Polytechnic Institute of Toulouse in March 2009. He is currently at the Institute of Electronics and Telecommunications of Rennes, France for a Post Doctoral position.

Mathieu Dervin was born in Paris in 1977. He received the Eng. degree in 2000 and the Ph.D. degree in Electronic and Communication Engineering in 2005, both from the Ecole Nationale Supérieure des Télécommunications (ENST) in Paris. Since 2006, he has been with the research department of Thales Alenia Space, Toulouse, France. He is carrying out technical studies to prepare the future space telecommunication systems. His research interests cover advanced digital communication techniques applied to the satellite transmissions, and include waveform and receiver architecture design.

Xavier Deplancq gets his Telecom Engineering degree from ENST Paris in 2004. He has been involved in development and testing of DVB-S2 receivers and transmitters (prototypes). He is also Telecom Performances Manager in Italian/French dual Telecom ATHENA-FIDUS program. He is also conducting many Research and Development activities in Signal Processing and Telecommunications. He is the Technical Responsible of the Transmission System Bench for Evaluation of Future Space Telecom solutions.